Journal of Applied Polymer Science

Synthesis and Characterization of s-Histidine-Derived Poly (ionic Liquid)/Silica Nanocomposites and Their Application in the Enantioselective Hydrolysis of a Chiral Ester

E. Kowsari,[1] S. M. Hosseini,[2] M. B. Bakhshandeh,[1] E. Ghrehkhani[2]

[1]Department of Chemistry, Amirkabir University of Technology, 424 Hafez Avenue, Tehran 1591634311, Iran

[2]Department of Chemistry, Islamic Azad University, Saveh, Iran

Correspondence to: E. Kowsari (E-mail: kowsarie@aut.ac.ir)

ABSTRACT: In this study, a new optically active monomer containing two chemically preformed imide rings was synthesized. The monomer was then used to synthesize optically active poly(amide imide)s (OAPAIs) and an optically active polyionic liquid (OAPIL), which were finally reacted with various amounts of silica nanoparticles in an *in situ* polymerization reaction to produce OAPAI/SiO_2 and OAPIL/SiO_2 hybrid materials containing sulfonic acid groups. The prepared monomers and the OAPAI and OAPIL nanocomposites were characterized by ^{1}H-NMR spectroscopy, Fourier transform infrared spectroscopy, thermogravimetric analysis, X-ray diffraction, scanning electron microscopy, X-ray photoelectron spectroscopy, and differential scanning calorimetry. OAPIL/SiO_2 served as an excellent catalyst in water as a solvent for the hydrolysis of D,L-phenylglycine methyl ester with the advantage of a markedly enhanced enantioselectivity and activity. Also, the enantioselectivity was strongly dependent on the SiO_2 content in the OAPIL/SiO_2 systems; a favorable SiO_2 content was 20% (w/w). The enantioselectivity was 95.2% (substrate conversion = 62.3%). © 2013 Wiley Periodicals, Inc. J. Appl. Polym. Sci. 000: 000–000, 2013

KEYWORDS: composites; functionalization of polymers; ionic liquids; nanostructured polymers; optical properties

Received 14 February 2013; accepted 27 May 2013; Published online 00 Month 2013

DOI: 10.1002/app.39595

INTRODUCTION

Optically active D-amino acids are widely used as intermediates in the pharmaceutical field for the production of semisynthetic antibiotics, peptides, hormones, and pesticides. Among them, D-phenylglycine (D-PG) and D-*p*-hydroxyphenylglycine are used as side chains for semisynthetic penicillins and cephalosporins, such as ampicillin and amoxicillin. The demand for these two amino acids will increase because they are also used for the production of drugs such as aspoxicillin and cefbuperazone.[1–5] In addition, several D-PG derivatives have been used as potent and selective antagonists of the ionotropic glutamate receptor.[6] L-Phenylglycine (L-PG) and its derivatives also play a crucial role in the synthesis of HIV protease inhibitors and taxol, a highly potent cancer drug.[7]

There are a variety of resolution techniques by which enantiomers are separated. Each method introduces an asymmetric environment either intramolecularly, in which a diastereomeric pair is chemically produced to interact with a nonchiral medium, or intermolecularly, where the underivatized free acid interacts with a chiral medium.[8–16] For each method, several advantages and disadvantages prevail, depending on factors such as time, purity, chemical processing, and inherent side reactions. These factors have all contributed to the lack of a universal enantiomeric separation regime for racemic phenylglycine. The most common method to date for the enantiomeric resolution of enantiomers and, in general chiral materials, is high-performance liquid chromatography (HPLC).[17–23] The construction of a chiral stationary phase or prederivatization of the individual enantiomers to produce a diastereomeric pair are two important techniques that have been used. Although these techniques vary from normal to reverse phase and use a variety of detector systems, the separations achieved thus far are similar. The disadvantage of this method is that there appears to be no universal chiral column or analysis conditions. In addition, large volumes of the organic-based mobile phase are required for component elution, and this volume of solvent must be evaporated to recover the free acid of phenylglycine. Another method of producing enantiomerically pure L-PG is selective enzymatic esterification with lipases.[24–27] The disadvantages of this method are related to the number of system parameters that must be optimized for the enzyme, and the selectivity of

Additional Supporting Information may be found in the online version of this article.

the system is limited by the extent of conversion.[28] Polyionic liquids (PILs), also called *polymeric* or *polymerized ionic liquids,* have an enabling role in some fields of polymer chemistry and material science. PILs have attracted considerable attention recently because they combine some unique characteristics of ionic liquids (ILs) with common properties of polymers, such as processability, durability, and mechanical stability. This makes PILs a class of versatile polymers for a multitude of applications, for instance, as solid ion conductors, CO_2 sorbents, dispersants, porous materials, and carbon precursors.[29–31] The self-assembly of PILs has received special interest because of the potential applications as a nanostructured functional material.[32] Recently, hierarchical nanocomposites have drawn considerable interest from chemistry and materials scientists. Among these types of nanocomposites, the binding of metal catalysts to inorganic or organic polymer supports has been widely used.[33,34] The development of novel materials and nanocomposites for chiral recognition has become increasingly important because of the significance of chiral separation, especially in the field of life sciences.[35,36]

In this study, new optically active polyionic liquid (OAPIL)/SiO_2 nanocomposites with different amounts of SiO_2 were synthesized. These OAPIL/SiO_2 nanocomposites were successfully used for the hydrolysis of D,L-phenylglycine methyl ester (D,L-PGME) with the advantage of a markedly enhanced enantioselectivity and activity. Furthermore, the effect of the SiO_2 content was examined. The addition of a suitable amount of SiO_2 improved the enantioselectivity.

EXPERIMENTAL

Materials

4,4′-Oxydianiline (97%), pyromellitic dianhydride (98%), *s*-histidine monohydrochloride monohydrate (98%), 4-methyl-1,3-phenylenediamine (98%), 1,5-naphthalenediamine (97%), 1,4-phenylenediamine (97%), 4,4′-(hexafluoroisopropylidene)-bis(4-phenoxyaniline), *N*-methyl-2-pyrrolidone (NMP; 99.5%), triphenyl phosphite (TPP; 98%), methanol (98%), tetraethoxysilane (TEOS; 99.9%), ammonium hydroxide (25%), and absolute ethanol (99%) were obtained from Merck Co. Racemic phenylglycine methyl ester (D-PGME), D,L-PGME, L-phenylglycine methyl ester (L-PGME), D-PG, and L-PG were purchased from Aldrich.

Measurements

^{1}H-NMR (500-MHz) spectra were recorded on a Bruker Avance 500 instrument (Rheinstetten, Germany). Fourier transform infrared (FTIR) spectra were recorded on a Jasco-680 spectrometer (Japan). The spectra of the solids were acquired with KBr pellets. The inherent viscosity was measured by a standard procedure with a Cannon-Fenske routine viscometer (Mianz, Germany). Thermogravimetric analysis (TGA) of the polymers was performed on a TGA 7 PerkinElmer (Jugeshin, Germany) in a nitrogen atmosphere at a rate of 10°C/min. Differential scanning calorimetry (DSC) analyses were performed on a Mettler DSC-30 under a nitrogen atmosphere. The morphology of the poly(amide imide) (PAI)/SiO_2 nanocomposite powders during milling was investigated by means of scanning electron microscopy (SEM; Philips, XL30) on gold-coated powders. The X-ray diffraction (XRD) patterns were recorded with a Philips X'Pert MPD diffractometer equipped with Cu Kα radiation ($\lambda = 1.54$ Å) in the range 10–80° at a speed of 0.05°/min. X-ray photoelectron spectra (XPS) were recorded on a PHI Quantera SXM spectrometer with a monochromated Al Kα X-ray source.

The initial rate (V_0), the enantiomeric excess (EE) of the residual substrate, and the substrate conversion (c) were calculated from the High-performance liquid chromatography (HPLC) analysis of the sample on a chiral Crownpak CR (+) column (4 × l50 mm^2, Daicel Chemical Industries, Ltd., Japan) with a Waters 600 pump and a Waters 996 photodiode array detector at 218 nm. The mobile phase was an aqueous solution of $HClO_4$ (35 mM, pH 1.6) at 0.8 mL/min. The retention times for D-PG, D-PGME, L-PG, and L-PGME were 3.05, 6.40, 9.70, and 18.46 min, respectively. The average error for this determination was less than 0.5%.

Monomer Synthesis

Into a 50-mL, round-bottomed flask were placed 0.324 g (1.5 mmol) of pyromellitic dianhydride, 0.63 g (0.629 mmol) of *s*-histidine monohydrochloride monohydrate (2), 30 mL of acetic acid, and a stirring bar. The mixture was stirred at room temperature for 3 h and was then refluxed for 8 h. The solvent was removed under reduced pressure, and 5 mL of cold concentrated HCl was added to the residue. A pale yellow precipitate was formed, filtered off, and washed with cold water.

Synthesis of Optically Active Poly(amide imide) (OAPAIs)/SiO_2 and OAPIL/SiO_2 Nanocomposites

A mixture of the diacid monomer (0.12 g, 0.2 mmol), a diamine (0.2 mmol), TPP (0.25 mL), and the IL (0.5 g) were placed in a 50-mL, round-bottomed flask and was heated. SiO_2 nanoparticles (20, 40, and 50%) were dispersed in 0.5 g of the IL and added to the monomer solutions. The mixture was heated with constant stirring at 180°C for 6 h. After 10–15 min of the reaction, the viscosity of the reaction mixture increased. After completion of the reaction, the highly viscous polymer solution was poured dropwise into a large amount of methanol (400 mL) with constant stirring. The off-white precipitates of the polymer were filtered and washed thoroughly with methanol followed several times by distilled water for the complete removal of the adsorbed IL. The polymers were dried overnight in an oven at 65°C *in vacuo* to remove all traces of the solvent (Scheme 1). The other OAPILs were prepared by the same procedure, but H_2SO_4 was added (Scheme 2).

Synthesis of SiO_2 Nanoparticles

The SiO_2 nanoparticles used in the nanocomposite synthesis were prepared by the acidic IL-templated sol–gel method. First, the pH of deionized water was adjusted to 7 with 30 wt % NH_3 in water and 0.1 g of the acidic IL 1-alkyl-3-methylimidazolium hydrogen sulfate ($[C_8mim]HSO_4$)[34] at 50°C. Next, 1.0 mL of TEOS and 0.1 g of the acidic IL $[C_8mim]HSO_4$[34] were added. After 2 h of reaction, the sample was then centrifuged and washed thoroughly with distilled water and ethanol. The acidic ionic liquid (AIL) templates were removed by extraction in acidic methanol (2 mL of HCl/100 mL of methanol, 36 h) at 343 K, and the surfactant-removed Mesoporous Silica Nanoparticles (MSNs) were centrifuged, washed several times with methanol, and dried *in vacuo* for 20 h. The resulting white powder was calcined in air for a period of 1 h at 650°C.

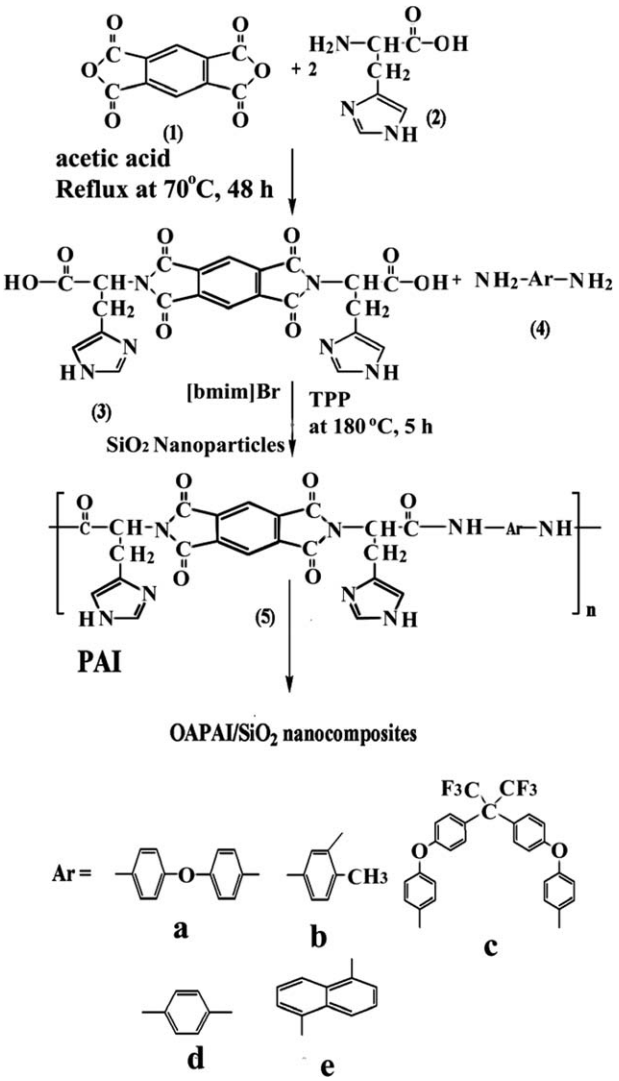

Scheme 1. Synthesis of the OAPAI/silica nanocomposites.

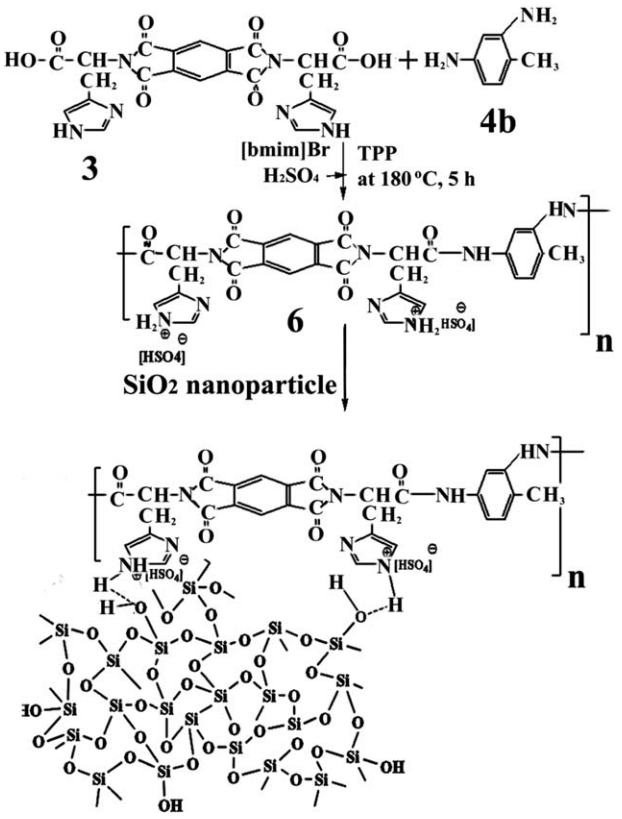

Scheme 2. Synthesis of the OAPIL/SiO_2 nanocomposite.

General Procedure for the Enantioselective Hydrolysis of D,L-PGME by OAPIL/SiO_2

D,L-PGME (0.16 mmol) was dissolved in 2 mL of double-distilled water, followed by the addition of 1.5 g of OAPIL/SiO_2 (20%). The reaction mixture was shaken in a water bath shaker at 150 rpm and 25°C. Aliquots (30 μL) were taken periodically from the reaction mixture and diluted with 250 μL of 0.2% v/v formic acid for HPLC analysis.

Inductively Coupled Plasma (ICP) Analysis

Sample preparation for ICP analysis was performed by coagulation of the OAPIL/SiO_2 nanocomposite with concentrated sulfuric acid. The remaining serum was used as the sample for injection into the ICP analyzer.

RESULTS AND DISCUSSION

Part One: Synthesis and Characterization of the *s*-Histidine-Derived OAPAIs and an OAPIL

Synthesis of the New Diacid-Containing Optically Active Moiety as a Monomer. Scheme 1 shows the synthesis of the diacid-containing optically active moiety. The dicarboxylic acid (compound **3**) was synthesized via the imidization of 2 equiv of *s*-histidine monohydrochloride in acetic acid as the solvent. In the first step, the mixture was stirred at room temperature to form an amic acid intermediate followed by imidization under refluxing conditions. FTIR spectroscopy and ^{1}H-NMR spectroscopy confirmed the structure of this compound. The FTIR spectrum showed absorption bands between 2950 and 3500 cm^{-1} (OH, carboxylic acid), 1750 cm^{-1} (imide C=O asymmetrical stretching), 1729 cm^{-1} (imide C=O symmetrical stretching), 1700 cm^{-1} (carboxylic acid C=O), and 1370 cm^{-1} (C—N stretching); this confirmed the presence of imide rings and carboxylic acid groups in the structure.

The ^{1}H-NMR spectrum showed a peak at 14.4 ppm, which was attributable to COOH protons, and peaks at 7.4–8.5 ppm, which were attributable to imidazole and benzene rings. These results clearly confirmed that the diacid **3** prepared herein was consistent with the proposed structure. Figure 1 shows the ^{1}H-NMR spectrum of the monomer diacid containing the optically active moiety.

Polymer Synthesis. ***Synthesis of OAPAIs.*** The OAPAIs were prepared by the direct polycondensation of five structurally different aromatic amines with the diacid monomer at a 1:1 molar ratio in an IL, 1-butyl-3-methylimidazolium bromide ([bmim]Br), as the solvent in the presence of TPP. A representative polycondensation mechanism is described in Scheme 1.

Synthesis of OAPIL. The OAPAIs were prepared by the direct polycondensation of aromatic amines (**4b**) with the diacid

Applied Polymer SCIENCE

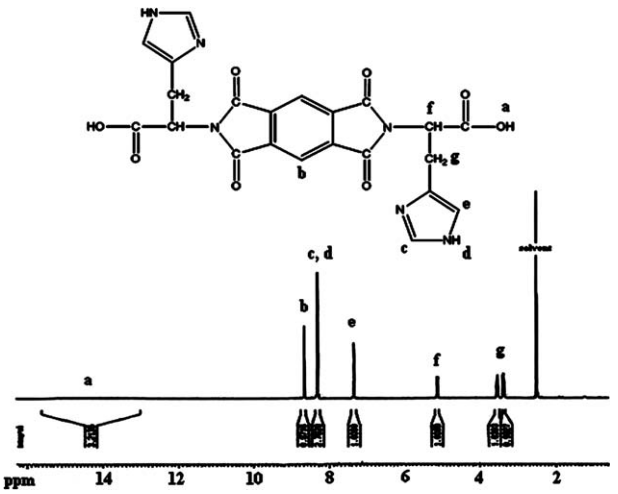

Figure 1. ^{1}H-NMR spectrum of the monomer.

monomer at a 1:1 molar ratio in an IL, [bmim]Br, as the solvent in the presence of TPP and H_2SO_4. A representative polycondensation mechanism is described in Scheme 2.

All of the OAPAIs and OAPILs showed optically active properties, and the specific rotations of these PAIs were measured in DMF at a concentration of 0.5 g/dL at 25°C in the range −53.10 to −78.3°. The chain structures were confirmed by IR and ^{1}H-NMR spectra. The FTIR spectra of the imide exhibited characteristic absorption bands around 1780 and 1370 cm^{-1} due to the C═O asymmetric, C═O symmetric, and C—N stretching of the imide ring. C—H stretching was shown as bands between 2950 and 3150 cm^{-1} and bands of the amide N—H appeared around 1610 and3300 cm^{-1}. The ^{1}H-NMR spectrum of OAPAIb exhibited similar patterns to the diacid monomer (**3**), and new signals at 8.30 and 9.50 ppm in the ^{1}H-NMR spectrum appeared; these were characteristic of phenyl amine and the amide N—H group. The ^{1}H-NMR spectrum of OAPAIb exhibited similar patterns to that of the related monomer. Figure 2 shows the ^{1}H-NMR spectrum of OAPAIb.

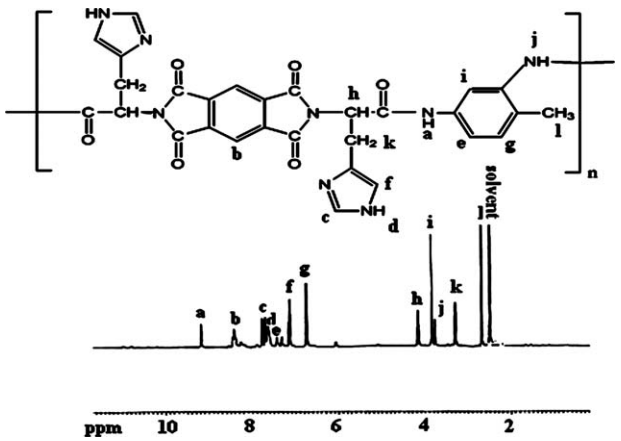

Figure 2. ^{1}H-NMR spectrum of OAPAIb.

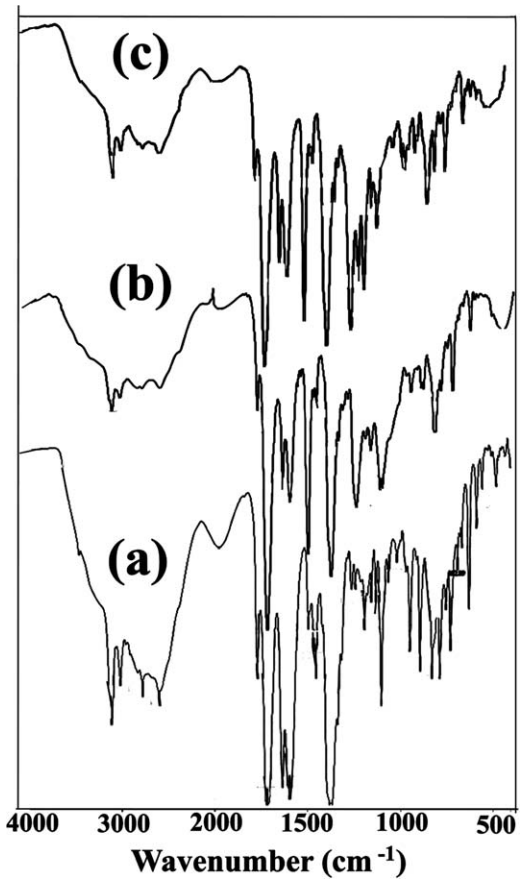

Figure 3. IR spectra of the nanocomposites: (a) OAPAId (40% silica), (b) OAPILb (40% silica), and (c) OAPAIc (40% silica).

FTIR Spectroscopy of the OAPAI/SiO_2 and OAPIL/SiO_2 Nanocomposites. The general features of the FTIR spectra of the OAPAI/SiO_2 and OAPIL/SiO_2 nanocomposites are shown in Figure 3. The spectra in Figure 3 and all the spectra throughout this study were normalized based on the intensity of the imide C═O stretching near 1770 cm^{-1}. The bands near 1378 and 730 cm^{-1} were attributed to C—N—C bonds and imide ring deformation, respectively. The discussion presented in the following text focuses on the N—H and the amide C═O regions, as these two regions contained the most important information on the interactions between the SiO_2 and PAI components. On the other hand, the intense and slightly broad peak at 1103 cm^{-1} (Si—O) showed the formation of a silica network.

The FTIR spectrum of OAPILb is depicted in Figure 3(b). The absorption of the SO group of the hydrogen sulfate ion (HSO_4^-) was observed as a broad band around 1176 cm^{-1} and a band around 1300 cm^{-1}.

Inherent Viscosity and Optical Activity of the Polymers. The inherent viscosities of all of the OAPAI and OAPIL samples were measured at a concentration of 0.5 g/dL in NMP with a viscometer at 25°C; the values are given in Table I. The inherent viscosity values of OAPAI and OAPIL were in the range 0.55–0.71 dL/g. The specific rotations of these OAPAI and OAPIL were measured in DMF at a concentration of 0.5 g/dL at 25°C in the range −53.10 to −78.3°.

Table I. Inherent Viscosity, Yield, and Rotation Values of the Optically Active Polymers

Polymer	Inherent viscosity (dL/g)[a]	Yield (%)	$[\alpha]_D^{25}$
OAPAIa	0.68	83	−53.1
OAPAIb	0.57	76	−75.4
OAPAIc	0.71	85	−48.3
OAPAId	0.55	72	−51.5
OAPAIe	0.61	78	−62.8
OAPILb	0.80	80	−78.3

[a] Measurement at a concentration of 0.5 g/dL in NMP at 25°C.

Thermal Properties. The thermal properties of OAPAI and OAPIL were studied by means of TGA and DSC at a heating rate of 10°C/min under a nitrogen atmosphere. The temperature at which the decomposition began was never under 200°C. Five thermal regions were selected on the TGA cures for the comparison of the thermal stabilities of the PAIs. These were the polymer decomposition temperature, the temperature at which a 10% weight loss occurred for the polymer, and the decomposition yield percentage (char yield at 900°C). The results are summarized in Table II.

The thermal behavior of the OAPAI/SiO_2 and OAPIL/SiO_2 nanocomposites were studied by TGA. All of the samples were heated in a nitrogen atmosphere from room temperature to 900°C at a heating rate of 10°C/min. Figure S1 in the Supporting Information shows the TGA curves of the OAPAI/SiO_2 nanocomposites OAPAIa, OAPAIc, and OAPAId. The residual

Table II. Thermal Properties of the PAI/Silica Nanocomposites

Nanocomposite	Silica content (wt %)	T_0 (°C)[a,d]	T_{10} (°C)[b]	T_{max} (°C)[c]	Char yield (%)[e]
OAPAId	20	275	350	825	12
	40	300	365	830	26
	50	350	450	880	30
OAPAIa	20	200	235	780	8
	40	285	250	800	11
	50	325	375	803	19
OAPAIc	20	180	203	715	33
	40	185	210	730	47
	50	200	250	750	54
OAPILb	20	210	260	718	35
	40	240	290	715	42
	50	260	310	730	53

[a] Initial decomposition temperature by TGA at a heating rate of 10°C/min in N_2.
[b] Temperature at which a 10% weight loss was recorded by TGA at a heating rate of 10°C/min in N_2.
[c] Maximum temperature degradation.
[d] T_g recorded at a heating rate of 10°C/min in N_2.
[e] Weight percentage of material left undecomposed after TGA at a maximum temperature of 900°C.

Table III. OAPAI–SiO_2-Catalyzed Enantioselective Hydrolysis of D,L-PGME in Water

	V_0 (mM/min)	Time (h)	c (%)	EEs (%)
OAPAIL-SiO_2 (20%)	2.86	0.5	53.3	95.2
OAPAIL-SiO_2 (40%)	2.25	1.0	46.4	62.7
OAPAIL-SiO_2 (50%)	2.21	1.0	46.4	62.7

The reactions were conducted in the double-distilled water (2 mL) containing 80 mM D,L-PGME and OAPAI-SiO_2 (2 g) at 25°C and 250 rpm.

weight of the sample was equivalent to the weight of the remaining carbon and silica after the decomposition process. Table III shows the effect of the various amounts of silica added to the reaction on the residual weight of the OAPAI/SiO_2 and OAPIL/SiO_2 nanocomposites, as determined by TGA. The results show that the residual weight increased slightly as the SiO_2 content increased (see Table III). This was clearly caused by the strong interaction between SiO_2 and the OAPAI, which limited the segmental movement of the PAI. It is thought that these materials would be good for particle applications.

Figure 4 shows the DSC curves for OAPAIa and OAPAIb. The data indicate that the glass-transition temperature (T_g) of pure OAPIL was higher than that of pure OAPAI. The main reason may have been the intermolecular hydrogen bonding of OAPIL.

SEM Micrographs of the OAPAI/SiO_2 and OAPIL/SiO_2 Nanocomposites. Figure 5 shows the SEM micrographs of the prepared OAPAI/SiO_2 and OAPIL/SiO_2 nanocomposites. In most cases, the surface morphology of materials is of great importance, as technical applications require a well-defined surface. No phase separation could be observed in Figure 5. That is, covalent bonding (Si—O—Si) between the materials enhanced the miscibility. In all of the samples, when the silica content was less than 20 wt %, the materials showed good miscibility between the polymer and silica phases, but when the silica content was increased to 40 or 50 wt %, the miscibility between the polymer and silica phase decreased.

The presence of hydroxyl groups and hydrogen bonding with HSO_4^- (from the IL, Scheme 2) on the surface of the silica nanoparticles increased the agglomeration tendency; this inversely influenced the particle dispersion in the polymer matrix. Moreover, the strength of the interaction between the organic and inorganic phases was the most important determining factor affecting the properties of the obtained materials (see Figure 6).

Powder XRD Analysis. The silica nanoparticles and PAI/SiO_2 nanocomposites were analyzed with powder XRD, the results of which are displayed in Figure 7. The XRD spectra of all of the samples showed the presence of an amorphous state. The presence of a crystallite phase in the PAI/SiO_2 nanocomposites could be explained by the formation of a silica network. The results show a completely amorphous structure in all of the samples with the addition of TEOS to the reaction.

XPS Analysis. XPS is a useful technique for monitoring polymer–polymer interactions in nitrogen-containing polymers.

Applied Polymer SCIENCE

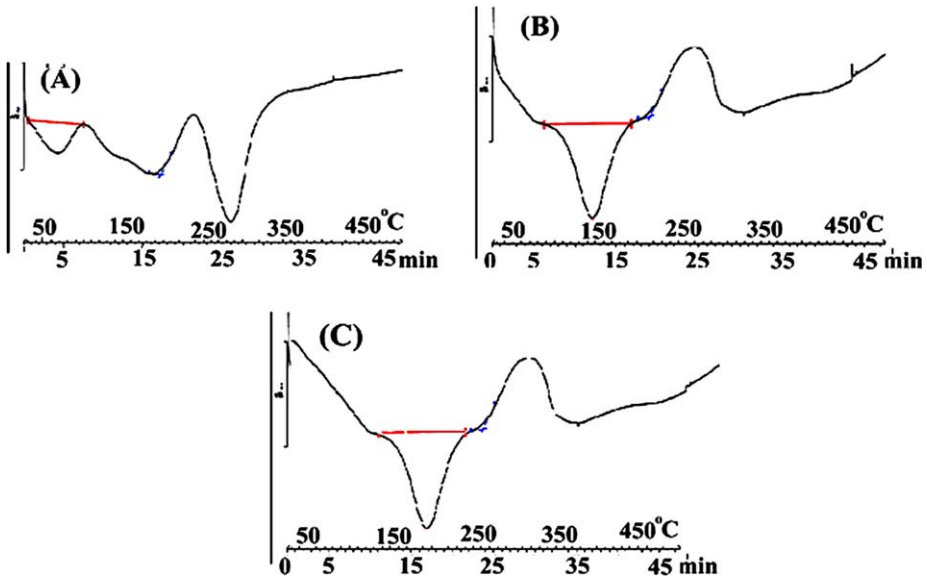

Figure 4. DSC spectra of (A) OAPAIa, (B) OAPAIb, and (C) OAPILb. [Color figure can be viewed in the online issue, which is available at wileyonlinelibrary.com.]

When the nitrogen atom is involved in hydrogen bonding, the binding energy of the N1s electron is increased by about 1.0 eV. Figure 8(b) shows the wide-scan spectrum of the pristine OAPAIa; only the expected components C, O, and N were found. Of these, the component peak at 284.8 eV in the C1s peak was attributed to the carbon atoms of the benzene rings of the PAI main-chain structure, and this was the criterion for correcting the binding energy scale. The O1s spectrum for pure

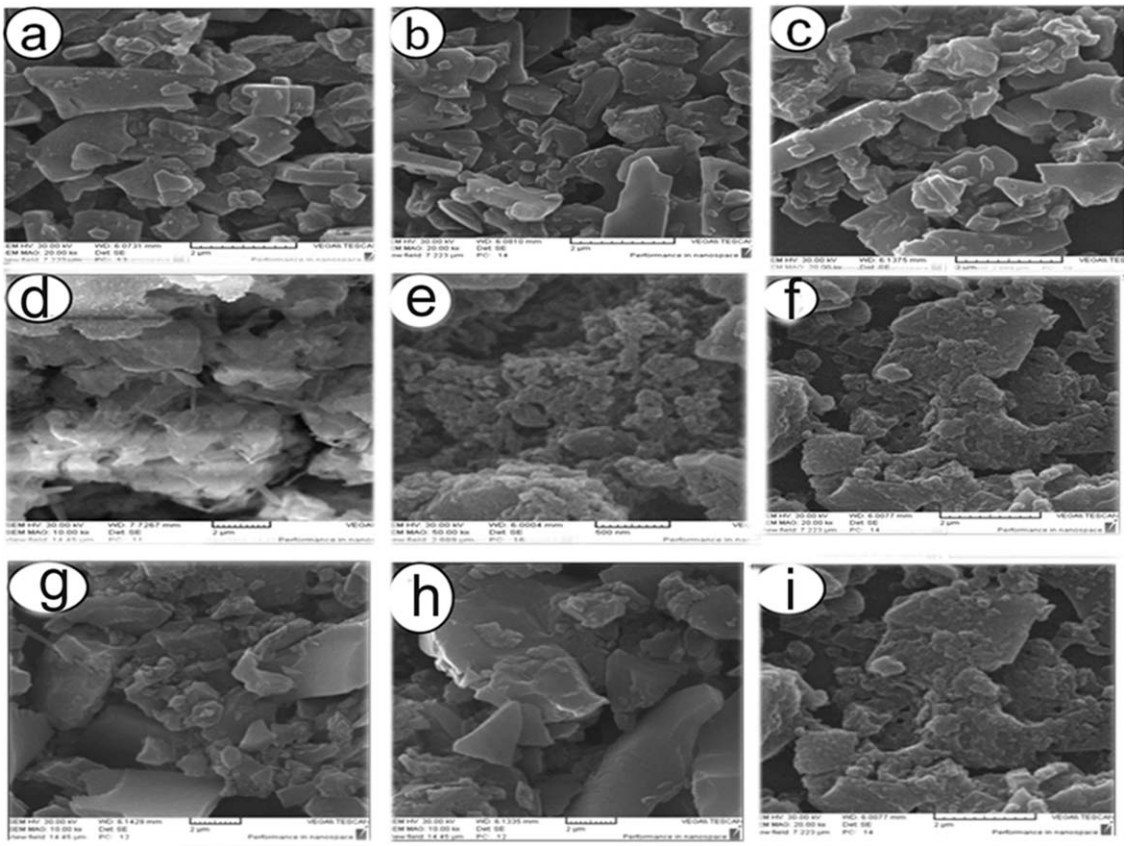

Figure 5. SEM micrographs of the nanocomposites: (a) OAPAId/SiO_2 (20%), (b) OAPAId/SiO_2 (40%), (c) OAPAId/SiO_2 (50%), (d) OAPAIa/SiO_2 (20%) silica, (e) OAPAIa/SiO_2 (40%), (f) OAPAIa/SiO_2 (50%), (g) OAPAIc/SiO_2 (20%), (h) OAPAIc/SiO_2 (40%), and (i) OAPAIc/SiO_2 (50%).

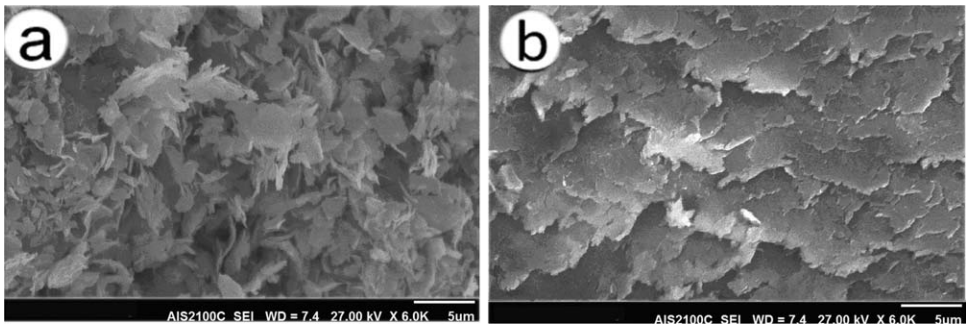

Figure 6. SEM micrographs of the OAPIL/SiO_2 nanocomposites: (a) 20 and (b) 40% silica.

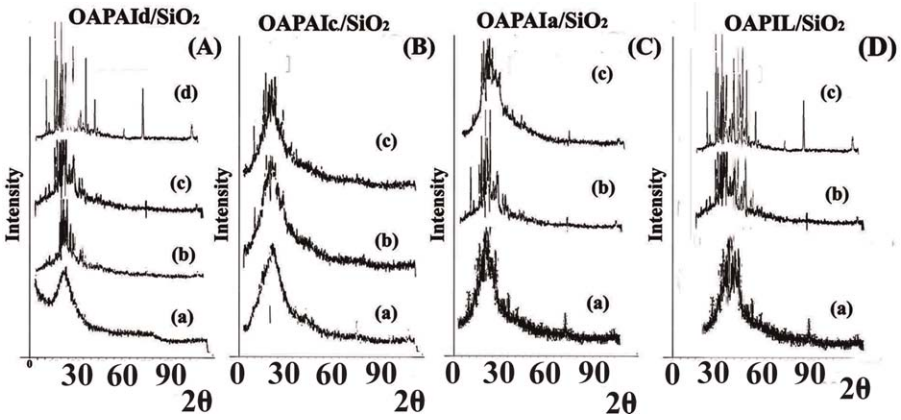

Figure 7. Powder XRD patterns of the (A) the OAPAId nanocomposite and silica nanoparticles [(a) XRD silica nanoparticles, (b) 20% silica, (c) 40% silica, and (d) 50% silica], (B) the OAPAIc nanocomposite [(a) 20, (b) 40, and (c) 50% silica], and (C) OAPAIa nanocomposite [(a) 20, (b) 40, and (c) 50% silica].

OAPAIa displayed two components with different relative intensities. The binding energy at 531.9 eV was attributed to the oxygen of the C═O bond, and the binding energy at 533.3 eV was attributed to a C—O—C bond.[37] The peak at 400.3 eV was assigned to the characteristic peak of nitrogen on a PAI backbone. Figure 8(a) shows the scan spectrum of SiO_2 nanoparticles. The Si 2p core-level spectrum showed a single peak at a binding energy of 103.5 eV, which was attributed to the formation the Si—O—Si network structure of SiO_2. The results were consistent with the FTIR analysis results.

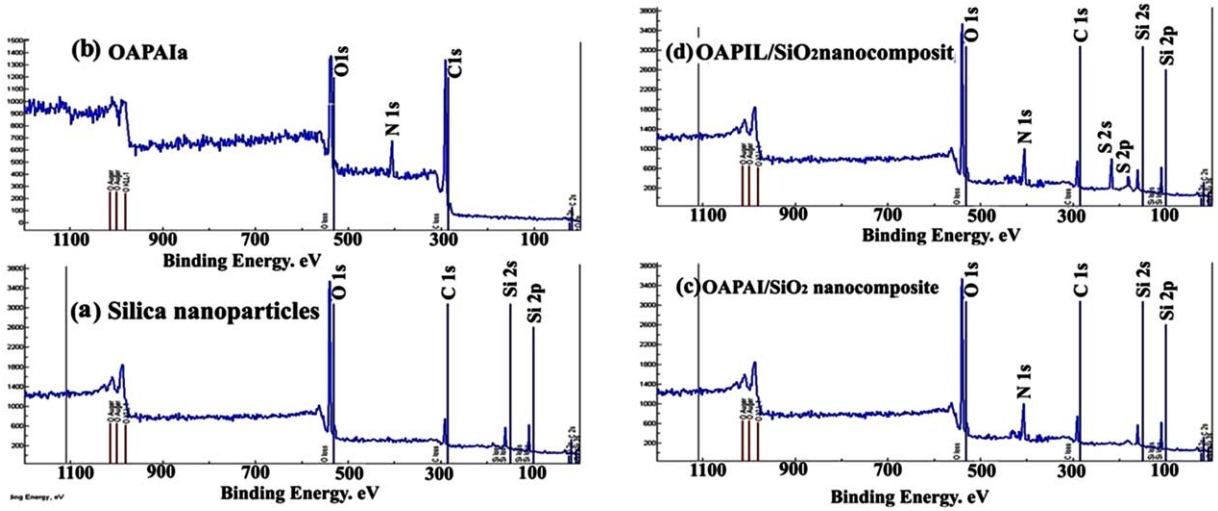

Figure 8. XPS spectra: (a) SiO_2 nanoparticles, (b) OAPAIa, (c) OAPAIa/SiO_2 (20%) nanocomposite, and (d) OAPIL/SiO_2 (20%) nanocomposite. [Color figure can be viewed in the online issue, which is available at wileyonlinelibrary.com.]

Applied Polymer SCIENCE

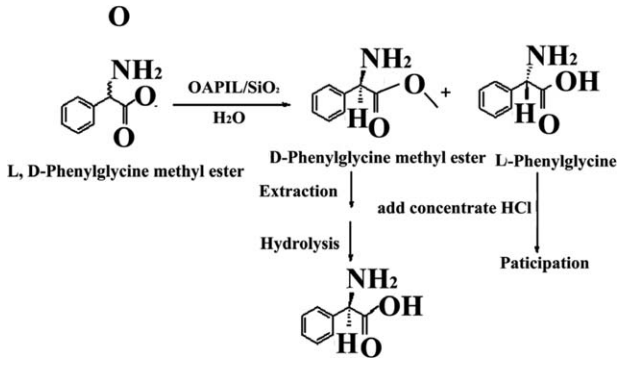

Scheme 3. Enantioselective hydrolysis of D,L-PGME by OAPIL/SiO_2.

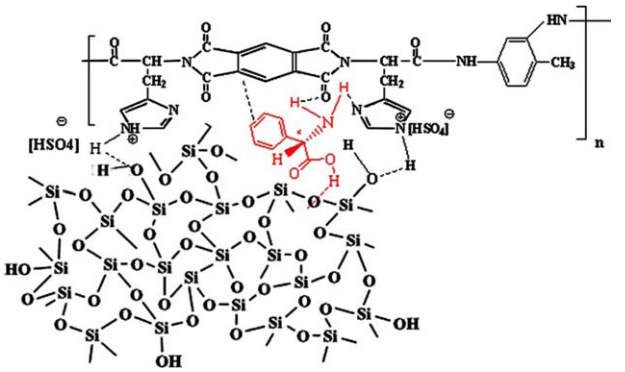

Scheme 4. Proposed models of the chiral discrimination on OAPIL/SiO_2 with L-PG. [Color figure can be viewed in the online issue, which is available at wileyonlinelibrary.com.]

Part Two: Application of OAPIL/SiO_2 to the Enantioselective Hydrolysis of D,L-PGME

Enantioselective Hydrolysis of D,L-PGME by OAPIL/SiO_2. Chemoenzymatic synthesis of L-PG with the hydantoinase of *Pseudomonas desmolyticum* resting cells was carried out by Gokhale et al.[38] This pure product was further chemically converted to D(−)-phenylglycine with nitrous acid with an 80% chemical yield. Thus, the overall conversion efficiency of D−5-phenylhydantoin to D(−)-phenylglycine was found to be 65–68%.

Enantiomer separation of *n*-protected α-phenylglycine on a covalently immobilized cellulose, tris(3,5-chlorophenylcarbamate), chiral stationary phase in HPLC was carried out by Jin et al.[39] The enantiomeric purity of phenylglycine was found to be 55%.

The effects of spacers and organic modifiers on the normal-phase liquid chromatographic behavior of benzoyl-D,L-octyl-amine and benzoyl-D,L-amino acid isopropyl esters on diamide-type chiral stationary phases (CSPs) with *N*-(3,5-dimethylbenzoyl)-D-phenyl–glycine were investigated by Chen et al.[40]

We prepared modern IL-containing nanocomposites as highly enantioselective catalysts. The enantioselective hydrolysis of D,L-PGME by OAPAI/SiO_2 is shown in Scheme 3. The optimum pH, substrate concentration, reaction temperature, and shaking rate were 8.0, 80 m*M*, 25–30°C, and 150 rpm, respectively, for OAPIL/SiO_2 (20%), under which V_0, the residual substrate EE, and the enantioselectivity were 2.35 m*M*/min, 95.2% ($c = 62.0\%$), and 40, respectively.

Table IV. The results obtained from ICP analysis for determination of silica content

	Measured amount of SiO_2 in serum (ppm)	Initial amount of SiO_2 (ppm)	Amount of free SiO_2 (wt %)
OAPAIL-SiO_2 (20%)	22,080	80,000	27.6
OAPAIL-SiO_2 (40%)	61,280	160,000	38.3
OAPAIL-SiO_2 (50%)	90,400	200,000	45.2

Add in each batch (theoretical).

The enantioselectivity of OAPIL/SiO_2 was strongly influenced by the weight percentage of SiO_2 (see Table III). In addition, OAPAI/SiO_2 dramatically lost hydrolytic activity with an increased weight percentage of SiO_2, and this led to poor enantioselectivity.

ICP analysis showed the presence and amount of silica nanoparticles in OAPAI–SiO_2. Through this preparative method, the amount of free silica during polymerization was measured. This gave us a good estimation of the OAPAI–SiO_2 nanocomposite; the results are shown in Table IV. We observed that the amount of free silica in the serum phase was not significant. This confirmed the progress of polymerization on the surface of the silica particles.

The results reported here clearly demonstrate that enantioselective catalysis in IL-containing systems is an exciting and burgeoning research area, which holds tremendous potential for opening up a new field of aqueous enantioselective catalysis. It is, therefore, worth further detailed investigations to gain sufficient knowledge about the influence of chiral ionic polymers on enantioselective catalysis.

Models of Chiral Recognition on OAPIL. As shown in Scheme 4, the general chiral recognition on OAPIL/SiO_2 is based on a two-point interaction. In the model, there are two hydrogen associations in the diastereomeric selector–solute complexes, the aromatic π–π interaction between the phenyl moieties and the steric effect of stereogenic center mediates chiral recognition. This is based on the consideration that the interactions between the phenyl or H on one stereogenic center with an R or H on the second seem unlikely because of the distance involved. A face-to-face approach promoted by the stacking of amide π–π poles in the model may explain the chiral recognition.

CONCLUSIONS

An optically active monomer containing two preformed imide cycles and two terminal carboxylic groups was prepared and characterized by ^{1}H-NMR spectroscopy. The monomer was then used to prepare a set of five OAPAI and three OAPAI/SiO_2 and OAPIL/SiO_2 catalysts, which were formed with an *in situ*

polymerization process with the addition of SiO_2 nanoparticles. OAPIL/SiO_2 (20%) served as an excellent catalyst in water as a solvent for the hydrolysis of D,L-PGME with the advantage of a markedly enhanced enantioselectivity and activity. The enantioselectivity was 95.2% ($c = 62.3\%$). ICP analysis showed that the amount of free silica in the serum phase was not significant, and this confirmed the progress of polymerization on the surface of the silica particles. Work is now in progress on extending this new methodology to the asymmetric hydrolysis of other useful amino acid methyl esters.

ACKNOWLEDGMENTS

The authors sincerely thank the Iranian Nanotechnology Initiative Council for its financial support.

REFERENCES

1. Bommarius, A. S.; Schwarma, M.; Drauz, K. *J. Mol. Catal. B* **1998**, *5*, 1.
2. Hubbard, B. K.; Thomas, M. G.; Walsh, C. T. *Chem. Biol.* **2000**, *7*, 931.
3. Lou, W. Y.; Zong, M. H.; Liu, Y. Y.; Wang, J. F. *J. Biotechnol.* **2006**, *125*, 64.
4. Bruggink, A.; Roos, E. C.; de Vroom, E. Org. Proc. Rev. Dev. **1998**, *2*, 128.
5. Arcuri, M. B.; Antunes, O. A. C.; Sabino, S. J.; Pinto, G. F.; Oestreicher, E. G. *Amino Acids* **2000**, *19*, 477.
6. Garcia, M. J.; Azerad, R. *Tetrahedron: Asymmetry* **1997**, *8*, 85.
7. Wang, Z. M.; Kolb, H. C.; Sharpless, K. B. *J. Org. Chem.* **1994**, *59*, 5104.
8. Jin, J. Y.; Lee, W.; Park, J. H.; Ryoo, J. J. *J. Liq. Chromatogr. Relat. Technol.* **2006**, *29*, 1793.
9. Jin, J. Y.; Lee, W.; Park, J. H.; Ryoo, J. J. *J. Liq. Chromatogr. Relat. Technol.* **2007**, *30*, 1.
10. Ali, I.; Aboul-Enein, H. Y. *J. Sep. Sci.* **2006**, *29*, 762.
11. Ghanem, A. *J. Sep. Sci.* **2007**, *30*, 1019.
12. Instruction Sheet for Chiral Technologies Laboratory Products: CHIRALPAK IC; Daicel Chemical Industries: Tokyo, **2007**.
13. Greene, T. W.; Wuts, P. G. M. Protective Groups in Organic Synthesis, 3rd ed.; Wiley: New York, **1999**.
14. Pirkle, W. H.; Lee, W. *Bull. Korean Chem. Soc.* **1998**, *19*, 1277.
15. Li, Y. H.; Baek, C. S.; Jo, B. W.; Lee, W. *Bull. Korean Chem. Soc.* **2005**, *26*, 998.
16. Bodansky, M.; Bodansky, A. The Practice of Peptide Synthesis; Springer: New York, **1984**.
17. Okamoto, Y.; Yashima, E. *Angew. Chem. Int. Ed.* **1998**, *37*, 1020.
18. Yashima, E. *J. Chromatogr. A* **2001**, *906*, 105.
19. Oi, N.; Kitahara, H.; Aoki, F.; Kisu, N. *J. Chromatogr. A* **1995**, *689*, 195.
20. Zhang, T.; Kientzy, C.; Franco, P.; Ohnishi, A.; Kagamihara, Y.; Kurosawa, H. *J. Chromatogr. A* **2005**, *1075*, 65.
21. Ghanem, A.; Hoenen, H.; Aboul-Enein, H. Y. *Talanta* **2006**, *68*, 602.
22. Ghanem, A.; Naim, L. *J. Chromatogr. A* **2006**, *1101*, 171.
23. Zhang, T.; Nguyen, D.; Franco, P.; Murakami, T.; Ohnishi, A.; Kurosawa, H. *Anal. Chim. Acta* **2006**, *557*, 221.
24. Wegman, M. A.; Hacking, M. A. P. J.; Rops, J.; Pereira, P.; van Rantwijk, F.; Sheldon, R. A. *Tetrahedron: Asymmetry* **1999**, *10*, 1739.
25. Du, W.; Zong, M. H.; Guo, Y.; Liu, D. H. *Biotechnol. Lett.* **2003**, *25*, 461.
26. Machado, G. D. C.; Gomes, M.; Antunes, O. A. C.; Oestreicher, E. G. Proc. Biochem. **2005**, *40*, 3186.
27. Chen, S. T.; Huang, W. H.; Wang, K. T. *J. Org. Chem.* **1994**, *59*, 7580.
28. Chen, C. S.; Fujimoto, Y.; Girdaukas, G.; Sih, J. *J. Am. Chem. Soc.* **1982**, *104*, 7294.
29. David, M. *Prog. Polym. Sci.* **2011**, *36*, 1629.
30. Green, O.; Grubjesic, S.; Lee, S.; Firestone, M. A. *Polym. Rev.* **2009**, *49*, 339.
31. Lu, J.; Yan, F.; Texter, J. *Prog. Polym. Sci.* **2009**, *34*, 431.
32. Grubjesic, S.; Seifert, S. N.; Firestone, M. A. *Macromolecules* **2009**, *42*, 5461.
33. Mahdavian, A. R.; Ashjari, M.; Bayat Makoo, A. *Eur. Polym. J.* **2007**, *43*, 336.
34. Kowsari, E.; Faraghi, G. *Ultrason. Sonochem.* **2010**, *17*, 718.
35. Berthod, A. *Anal. Chem.* **2006**, *78*, 2093.
36. Ward, T. J. *Anal. Chem.* **2006**, *78*, 3947.
37. Jordan, J.; Jacob, K. I.; Tannenbaum, R.; Sharaf, M. A.; Jasiukd, I. *Mater. Sci. Eng.* **2005**, *393*, 1.
38. Gokhale, D. V.; Bastawde, K. B.; Patil, S. G.; Kalkote, U. R.; Joshi, R. R.; Joshi, R. A.; Ravindranathan, T.; Gaikwad, B. G.; Jogdand, V. V.; Nene, S. *Enzyme Microb. Technol.* **1996**, *18*, 363.
39. Jin, J. Y.; Lee, W. *Bull. Korean Chem. Soc.* **2008**, *29*, 491.
40. Chen, Z.; Fuyumuro, T.; Watabe, K.; Hobo, T. *Anal. Chim. Acta* **2004**, *518*, 181.